

Avrami exponent of crystallization in tellurite glasses

S. M. Sidel · F. A. Santos · V. O. Gordo ·
E. Idalgo · A. A. Monteiro · J. C. S. Moraes ·
K. Yukimitu

CBRATEC7 Conference Special Issue
© Akadémiai Kiadó, Budapest, Hungary 2011

Abstract Nucleation process and crystal growth for three samples of the $(20-x)\text{Li}_2\text{O}-80\text{TeO}_2-x\text{WO}_3$ glass system were studied using X-ray diffraction and differential scanning calorimetry techniques. X-ray diffraction data confirmed the amorphous characteristic of the *as-quenched* samples and indicated the growth of crystalline phases formed due to the thermal treatment for annealed samples. These results reveal the presence of three distinct $\gamma\text{-TeO}_2$, $\alpha\text{-TeO}_2$ and $\alpha\text{-Li}_2\text{Te}_2\text{O}_5$ crystalline phases in the TL sample, and two distinct $\alpha\text{-TeO}_2$ and $\gamma\text{-TeO}_2$ crystalline phases in the TLW5 and TLW10 samples. The activation energy and the Avrami exponent were determined from DSC measurements. The activation energy values X-ray diffraction data of the TLW10 glass sample suggest that $\gamma\text{-TeO}_2$ phase occur before the $\alpha\text{-TeO}_2$. The results obtained for the Avrami exponent point to that the nucleation process is volumetric and that the crystal growth is two or three-dimensional.

Keywords Tellurite glasses · Nucleation · Crystallization · Activation energy · XRD · DSC

Introduction

With the advent of the lasers, mainly the pulsed lasers, vitreous materials have attracted considerable interest for

applications in the communication and in the photonics devices, especially in the non-linear optics. Currently, the objective of the research is to substitute electronic systems by optical devices with objective to use the light in the transmission, modulation, amplification, and information storage [1, 2]. Vitreous matrices based on tellurite glasses (TeO_2) [3, 4] present a third harmonic generation (χ^3) with approximately one order of magnitude higher than silicates and borates glasses.

Study of the thermal and structural properties [5, 6] of tellurite glasses is important to understand the nucleation and crystal growth mechanism which is essential to obtain high quality glasses for technological applications. Many works have reported the glass thermal properties studied by isothermal and non-isothermal methods [7, 8]. The non-isothermal method offers some advantages when compared to isothermal method. One of them is that the non-isothermal experiments can be performed in shorter time period and in a wider temperature range. In addition, most phase transformations occur too rapidly to be measured under isothermal conditions because of the inherent transients associated with the experimental apparatus [9, 10].

Structural properties studies reveal two stable crystalline forms for TeO_2 : $\alpha\text{-TeO}_2$ (paratellurite) [11] and $\beta\text{-TeO}_2$ (tellurite) [12]. The basic structure is constituted by the trigonal bipyramid (TeO_4), linked for vertexes in the $\alpha\text{-TeO}_2$ phase and for the edges in the $\beta\text{-TeO}_2$ phase. In addition, new crystalline polymorphic phases, $\delta\text{-TeO}_2$ and $\gamma\text{-TeO}_2$, were discovered [13, 14]. The $\gamma\text{-TeO}_2$ structure is constituted by a distorted TeO_4E bi-pyramid with one of the vertexes occupied for a pair of free electrons.

The purpose of this study was to study the nucleation and crystallization kinetic of the $\text{Li}_2\text{O}-\text{TeO}_2-\text{WO}_3$ glass system determining the activation energy and the Avrami

S. M. Sidel (✉) · F. A. Santos · V. O. Gordo · E. Idalgo ·
A. A. Monteiro · J. C. S. Moraes · K. Yukimitu
Faculdade de Engenharia, UNESP—Univ Estadual Paulista,
Ilha Solteira, SP, Brazil
e-mail: sidel@uft.edu.br

S. M. Sidel
UFT—Universidade Federal do Tocantins, Palmas, TO, Brazil

exponent from the formed crystalline phases due to heating treatment of the samples.

Materials and methods

The glasses of the $(20-x)\text{Li}_2\text{O}-80\text{TeO}_2-x\text{WO}_3$ system were prepared by the conventional melt-quenching method. The obtained samples are referred in the text as TL ($x = 0$ mol%), TLW5 ($x = 5$ mol%), and TLW10 ($x = 10$ mol%). The samples were obtained from the commercial reagents Li_2CO_3 (Aldrich, 99+%), TeO_2 (Aldrich, 99+%) and WO_3 (Aldrich, 99+%). These reagents in appropriated ratios were mixed to give 5 g batches. The mixture was melted in a platinum crucible using an electric furnace at 800 °C for TL glass and at 850 °C to the other two glasses for 30 min. The molten material was poured onto pre-heated brass mold and was immediately placed in other furnace for annealing. The samples were annealed at 200 °C for TL and 250 °C for TLW5 and TLW10 glasses during 2 h. These samples will be cited in the text *as-quenched*.

Thermal properties were studied by differential scanning calorimetry (DSC) technique carried out in a DSC 2920 equipment (TA Instruments). The DSC thermograms were obtained using 10 mg of sample enclosed in aluminum pan under dry nitrogen atmosphere for five different heating rates (2.5, 5.0, 7.5, 10.0, and 12.5 K min^{-1}). The crystallized glasses were analyzed by X-ray diffraction (XRD) technique using Cu $K\alpha$ radiation of a RU200B Rigaku equipment. Powder samples with particle size of 45–63 μm were used for DSC and XRD measurements.

The Johnson–Mehl–Avrami–Kolmogorov (JMAK) theory was used to determine the Avrami exponent (n) [15–17]. This theory describes the evolution in the time (t), or temperature (T), of the crystallized volume fraction (x) for non-isothermal process [18–21]. The n parameter was determined from the DSC data considering the following equation [9, 22]:

$$n = \left(\frac{dx}{dt} \right)_p \frac{RT_p^2}{0.37 \phi E} \quad (1)$$

where E is activation energy for the crystallization, T_p the temperature corresponding to the maximum of the DSC crystallization peak, R the gas constant, ϕ the heating rate, and $(dx/dt)_p$ the maximum crystallization rate. All thermograms were fitted using Gaussian functions to determine the crystallization peak temperature (T_p) corresponding to the phases observed in each glass sample. The E values were determined through the Kissinger relation [23, 24], $\ln(T_p^2/\phi) = E/RT_p$, considering the slope of the $\ln(T_p^2/\phi)$ versus $(1/T_p)$ curve.

The n value matches the nucleation type, if it is homogeneous or heterogeneous, and also the dimensionality of crystal growth. The $n = 1$ and $n > 1$ values indicate that the nucleation is superficial and volumetric, respectively. On the other hand, the crystal growth can be three- ($n = 4$), two- ($n = 3$), or one-dimensional ($n = 2$) [16, 17, 25–28].

There are others theoretical models to evaluate the crystallization mechanism of glasses such as Ozawa [29], Augis and Bennett [30], Vázquez et al. [31], Ray and Day [32], and Matusita et al. [25, 26]. In this work, the results obtained using the JMAK theories were compared with the Matusita model.

Results

Figure 1 shows XRD patterns of TL glass as-quenched (Fig. 1a) and heat annealed at different temperatures (Fig. 1b–e). In the Fig. 1a shows a typical amorphous characteristic which was maintained with also heat treatment at 548 and 597 K for 5 min, Fig. 1b and c, respectively. However, XRD pattern of the sample treated at 608 K for 5 min (Fig. 1d) shows a typical glass–ceramic XRD pattern where the indexed peaks were attribute to $\alpha\text{-TeO}_2$ and $\gamma\text{-TeO}_2$ crystalline phases. Finally, the XRD pattern of glass heat annealed at 634 K for 5 min (Fig. 1e) shows the presence of the $\alpha\text{-Li}_2\text{Te}_2\text{O}_5$ crystalline phase in coexistence with the $\alpha\text{-TeO}_2$ and $\gamma\text{-TeO}_2$ phases. The structure of the $\alpha\text{-TeO}_2$ phase is formed by a three-dimensional net of TeO_4 connected by asymmetric bridges of Te-O-Te and the structure of the $\gamma\text{-TeO}_2$ phase is

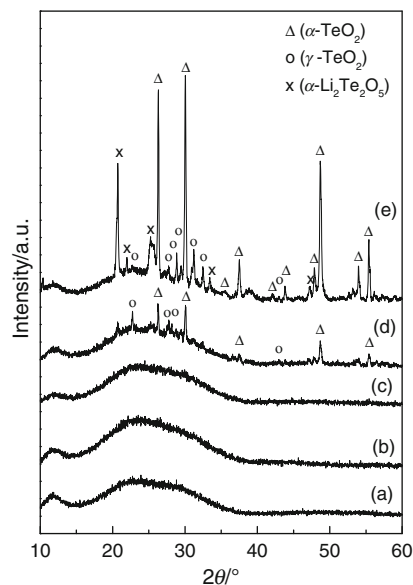
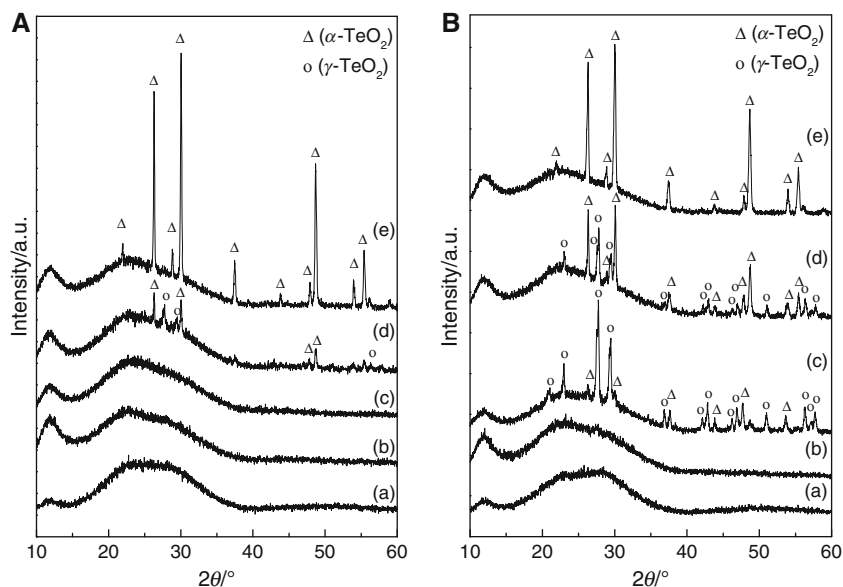


Fig. 1 X-ray diffraction patterns of the TL glass: (a) as-quenched and heat treated at (b) 548 K, (c) 597 K, (d) 608 K, and (e) 634 K for 5 min

Fig. 2 X-ray diffraction patterns. **A** TLW5 glass: (a) as-quenched and heat treated at (b) 553 K, (c) 643 K, (d) 653 K, and (e) 663 K; and **B** TLW10 glass: (a) as-quenched and heat treated at (b) 658 K, (c) 681 K, (d) 689 K, and (e) 713 K



formed by unities of TeO_4 alternately linked by almost symmetrical and highly asymmetric bridges of Te-O-Te [13, 14, 33].

XRD measurements also were performed for the TLW5 and TLW10 glasses and the results are showed in Fig. 2A and B, respectively. The XRD patterns of the as-quenched and heat treated samples at 553 and 643 K (Fig. 2A) and at 658 K (Fig. 2B) are typical of amorphous materials. On the other hand, the patterns of the treated samples at 653 K (Fig. 2A-d) and 663 K (Fig. 2A-e) for the TLW5 glass, and at 681 K (Fig. 2B-c), 689 K (Fig. 2B-d), and 713 K (Fig. 2B-e) for the TLW10 glass are characteristic of a vitro-ceramic and are associated the formation of the $\alpha\text{-TeO}_2$ and $\gamma\text{-TeO}_2$ crystalline phases. It is observed only the $\alpha\text{-TeO}_2$ crystalline phase for the TLW5 and TLW10 glasses heating treated at 663 and 713 K, respectively, suggesting a transition [12, 34, 35] from the $\gamma\text{-TeO}_2$ to the $\alpha\text{-TeO}_2$ crystalline phase. Furthermore, the XRD data of the TLW5 and TLW10 glasses indicate that the addition of WO_3 in the composition of the glass not allow the formation of the $\alpha\text{-Li}_2\text{Te}_2\text{O}_5$ crystalline phase.

Figure 3 shows DSC curves for heat flow versus temperature recorded at different heating rates. The T_g of all glasses were determined as indicated in the top insert of Fig. 3. The curves show the presence of exothermic peaks for each sample in different heating rates. The asymmetry observed in the crystallization peaks suggests the formation of different crystalline phases during the crystallization process. This is in agreement with XRD data. As mentioned above, were observed three crystalline phases ($\alpha\text{-TeO}_2$, $\gamma\text{-TeO}_2$, and $\alpha\text{-Li}_2\text{Te}_2\text{O}_5$) for the TL sample and of two crystalline phases ($\alpha\text{-TeO}_2$ and $\gamma\text{-TeO}_2$) for TLW5 and TLW10 samples. The crystallization peaks were fitted

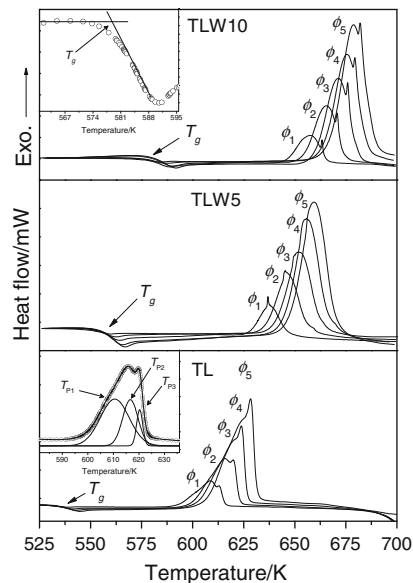


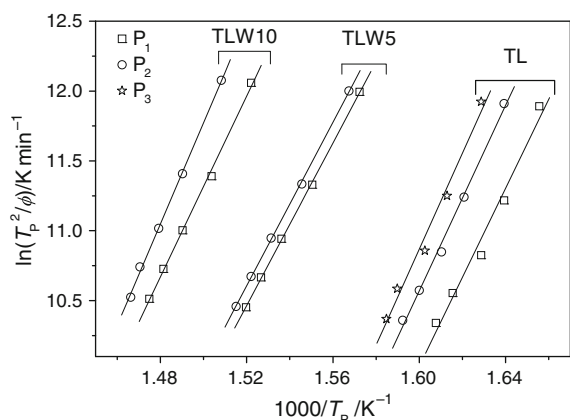
Fig. 3 DSC curves of the TL, TLW5, and TLW10 glasses recorded at different heating rates (ϕ)

using Gaussian functions considering the superposition of the crystalline phases. Thus, the maximum temperatures associated with the crystalline phases were obtained. As example, the bottom insert of Fig. 3 shows the three maximum temperatures (T_{P1} , T_{P2} , and T_{P3}) associated the three crystalline phases observed in the TL glass.

Table 1 summarizes the values of the T_g and T_P of the TL, TLW5, and TLW10 glasses for different heating rates. As can be observed, occurs a significant increase in the T_g value for the samples with WO_3 . This increase may be associated with decreasing of mobility in the glasses.

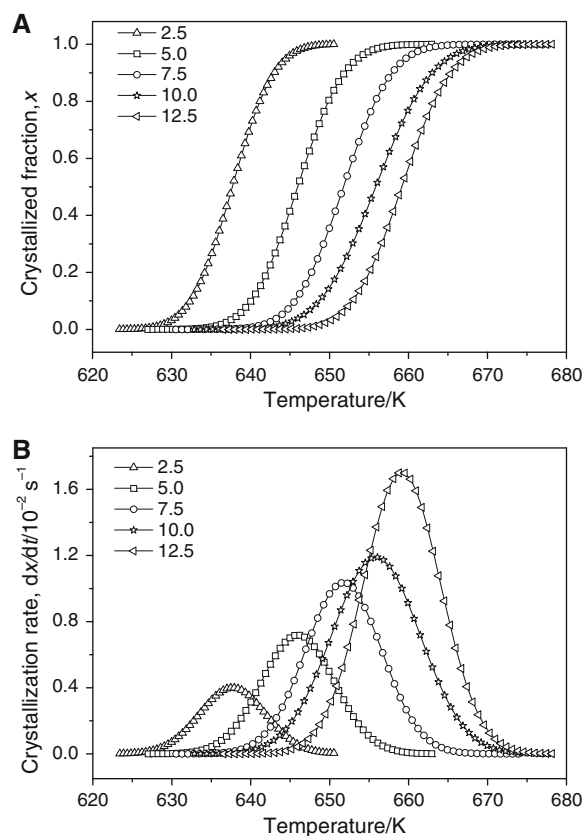
Table 1 Summary for temperature of crystallization peak from DSC curves recorded for TL, TLW5, and TLW10 glasses of 45–63 μm particles size at different heating rates

Heating rate $\phi/\text{K min}^{-1}$	TL glass				TLW5 glass			TLW10 glass		
	T_g/K	Peak temperature/K			T_g/K	Peak temperature/K		T_g/K	Peak temperature/K	
		T_{P1}	T_{P2}	T_{P3}		T_{P1}	T_{P2}		T_{P1}	T_{P2}
2.5	526	604	610	614	548	636	638	570	657	663
5.0	530	610	617	620	550	645	647	574	665	671
7.5	532	614	621	624	552	651	653	576	671	676
10.0	533	619	625	629	554	655	657	578	675	680
12.5	534	622	628	631	555	658	660	579	678	682

**Fig. 4** Kissinger plots for the crystallization peaks of the TL, TLW5, and TLW10 glasses

To obtain n values it is necessary calculate the activation energy (E) and maximum of crystallization rate curve $(dx/dt)_p$. First, the activation energies of the crystalline phases of each sample were determined from slope of the $\ln(T_p/\phi)$ versus $1/T_p$ curves (Fig. 4). On the other hand, the crystallization rate (dx/dt) it was determined from the crystallized volume fraction (x) as function of the temperature for the DSC crystallization peaks in different heating rates. The crystallized fraction at generic temperature T is given by $x = A/A_0$, where A_0 is total area between the T_i and T_f temperatures. T_i is the temperature where the crystallization is just beginning and T_f is the temperature where the crystallization is completed. The A is the partial area between T_i and T temperatures [7, 36]. The Fig. 5A shows the crystallized fraction in function of the temperature for the second crystallization peak of the TLW5 glass. The sigmoid form of the obtained curves is characteristic of volumetric crystallization. The curves of Fig. 5B represent the slope of crystallized fraction curves (Fig. 5A) with respect to the temperature and the maximum of these curves correspond to the $(dx/dt)_p$ values.

Therefore, the values $(dx/dt)_p$, T_p , R ($8.314 \text{ J mol}^{-1} \text{ K}^{-1}$), ϕ , and E were used to determine the n parameter using the

**Fig. 5** **A** Crystallized fraction (x) and **B** Crystallization rate (dx/dt) as function of the temperature (T) for second crystallization peak of the TLW5 glass at different heating rates

Eq. 1. The n and E values are summarized in the Table 2. The n values are the average between the values obtained for different heating rates. The n values indicate that the nucleation and the crystals growth take place through more than one mechanism. Thus, the results obtained by JMAK and Matusita models are in agreement and point to a volumetric nucleation with crystals growth occurring in two-dimensional ($\bar{n}_1 \approx 3$) followed by three-dimensional (\bar{n}_2 and $\bar{n}_3 > 4$) for TL glass, two-dimensional (\bar{n}_1 and $\bar{n}_2 \approx 3$) for

Table 2 E and n values associated to the crystallization peaks for three studied glasses

Glass	Activation energy, $E/\text{kJ mol}^{-1}$			Avrami exponent, n					
	E_1	E_2	E_3	JMAK			Matusita		
				\bar{n}_1	\bar{n}_2	\bar{n}_3	\bar{n}_1	\bar{n}_2	\bar{n}_3
TL	265 ± 9	276 ± 5	285 ± 8	2.8	3.8	5.3	2.8	3.7	5.8
TLW5	242 ± 1	243 ± 1	–	2.8	3.3	–	2.6	3.6	–
TLW10	269 ± 3	302 ± 3	–	2.8	4.0	–	2.4	4.3	–

TLW5 glass, and two-dimensional ($\bar{n}_1 \approx 3$) followed by three-dimensional ($\bar{n}_2 = 4$) for TLW10.

As in our previous work [37], the XRD data of the TL glass it not allow to know between $\gamma\text{-TeO}_2$ and $\alpha\text{-TeO}_2$ phases what of them takes place first. It is possible only to affirm that the $\alpha\text{-Li}_2\text{Te}_2\text{O}_5$ crystalline phase occurs after the $\gamma\text{-TeO}_2$ and $\alpha\text{-TeO}_2$ phases. The same occur with the TLW5 glass. For these two glasses no significant difference was observed in the activation energy. On the other hand, though it is not possible to affirm but the tendency observed in the XRD patterns and the E values obtained for TLW10 glass suggest that the $\gamma\text{-TeO}_2$ phase occur before than $\alpha\text{-TeO}_2$ phase.

Conclusions

The $(20-x)\text{Li}_2\text{O}-80\text{TeO}_2-x\text{WO}_3$ glasses were studied by XRD and DSC techniques to understand the nucleation and crystals growth process on these glasses. The results obtained with TL glass suggest that the $\text{Li}_2\text{Te}_2\text{O}_5$ crystallization occur after the $\gamma\text{-TeO}_2$ and $\alpha\text{-TeO}_2$. Furthermore, from XRD data and the E values obtained for TL and TLW5 glasses it does not allow to know what is the phase between $\gamma\text{-TeO}_2$ and $\alpha\text{-TeO}_2$ that crystallized first. On the other hand, the E values and XRD data for TLW10 glass suggest that the $\gamma\text{-TeO}_2$ occur before the $\alpha\text{-TeO}_2$. Finally, the Avrami exponents point to a volumetric nucleation with two-dimensional crystal growth followed by three-dimensional for TL and TLW10 glasses and only two-dimensional for TLW5 glass.

Acknowledgements The authors acknowledge the Brazilian agencies CNPq, CAPES and FAPESP for financial support.

References

- Shelby JE. Introduction to glass science and technology. Cambridge: The Royal Society of Chemistry; 1997.
- Tanaka K. Optical nonlinearity in photonic glasses. *J Mater Sci Mater Electron*. 2005;16:633–43.
- Yakhkind AK. Tellurite glasses. *J Am Ceram Soc*. 1966;49:670–8.
- Nasu H, Matsushita O, Kamiya K, Kobayashi H, Kubodera K. Third harmonic-generation from $\text{Li}_2\text{O}-\text{TiO}_2\text{-TeO}_2$ glasses. *J Non-Cryst Solids*. 1990;124:275–7.
- El-Mallawany RAF. Tellurite glasses. Part 1: elastic properties. *Mater Chem Phys*. 1998;53:93–120.
- El-Mallawany RAF. Tellurite glasses. Part 2: anelastic, phase separation, Debye temperature and thermal properties. *Mater Chem Phys*. 1999;60:103–31.
- Kuo MC, Huang JC, Chen M. Non-isothermal crystallization kinetic behavior of alumina nanoparticle filled poly (ether-ether ketone). *Mater Chem Phys*. 2006;99:258–68.
- Shaaban ER. Non-isothermal crystallization kinetic studies on a ternary, $\text{Sb}_{0.14}\text{As}_{0.38}\text{Se}_{0.48}$ chalcogenide semi-conducting glass. *Phys B*. 2006;373:211–6.
- Gao YQ, Wang W. On the activation energy of crystallization in metallic glasses. *J Non-Cryst Solids*. 1986;81:129–34.
- Henderson DW. Thermal analysis of non-crystallization kinetics in glass forming liquids. *J Non-Cryst Solids*. 1979;30:301–15.
- Thomas PA. The crystal structure and absolute optical chirality of paratellurite, $\alpha\text{-TeO}_2$. *J Phys C*. 1988;21:4611–27.
- El-Mallawany RAF. Tellurite glasses handbook: physical properties and data. Boca Raton: CRC Press; 2002.
- Champarnaud-Mesjard JC, Banchandin S, Thomas P, Mirgorodsky AP, Merle-Mérjean T, Frit B. Crystal structure, Raman spectrum and lattice dynamics of a new metastable form of tellurium dioxide: $\gamma\text{-TeO}_2$. *J Phys Chem Solids*. 2000;61:1499–507.
- Mirgorodsky AP, Merle-Mérjean T, Champarnaud-Mesjard JC, Thomas P, Frit B. Dynamics and structure of TeO_2 polymorphs: model treatment of paratellurite and tellurite; Raman scattering evidence for new γ - and δ -phases. *J Phys Chem Solids*. 2000;61:501–9.
- Johnson WA, Mehl RF. Reaction kinetics in processes of nucleation and growth. *Trans Am Inst Min Metal Eng*. 1939;135:416–42.
- Avrami M. Kinetics of phase change. I General theory. *J Chem Phys*. 1939;7:1103–12.
- Avrami M. Kinetics of phase change. II Transformation–time relations for random distribution of nuclei. *J Chem Phys*. 1940;8:212–24.
- Fokin VM, Zanotto ED, Yuritsyn NS, Schmelzer JWP. Homogeneous crystal nucleation in silicate glasses: a 40 years perspective. *J Non-Cryst Solids*. 2006;352:2681–714.
- Ma L, Li L, Guo C. Influence of m-isopropenyl-a, a-dimethylbenzyl isocyanate and styrene on non-isothermal crystallization behavior of polypropylene. *J Therm Anal Calorim*. 2010;101:1101–9.
- Kozmidis-Petrovic AF, Strbac GR, Strbac DD. Kinetics of non-isothermal crystallization of chalcogenide glasses from the $\text{Sb}_{32}\text{As}_5\text{S}_{48}\text{I}_{15}$ system. *J Non-Cryst Solids*. 2007;353:2014–9.
- Majhi K, Varma KBR. Crystallization kinetics of $\text{SrBi}_2\text{B}_2\text{O}_7$ glasses by non-isothermal methods. *J Therm Anal Calorim*. 2009;98:731–6.
- Araújo EB, Idalgo E. Non-isothermal studies on crystallization kinetics of tellurite $20\text{Li}_2\text{O}-80\text{TeO}_2$ glass. *J Therm Anal Calorim*. 2009;95:37–42.
- Kissinger HE. Variation of peak temperature with heating rate in differential thermal analysis. *J Res Natl Bureaun Stand*. 1956;57:217–21.
- Kissinger HE. Reaction kinetics in differential thermal analysis. *J Res Natl Bureaun Stand*. 1957;29:1702–6.
- Matusita K, Sakka S. Kinetics study of the crystallization of glass by differential scanning calorimetry. *Phys Chem Glasses*. 1979;20:81–4.

26. Matusita K, Komatsu T, Yokota R. Kinetics of non-isothermal crystallization process and activation-energy for crystal-growth in amorphous materials. *J Mater Sci.* 1984;19:291–6.
27. Long Y, Shanks RA, Stachurski ZH. Kinetics of polymer crystallization. *Prog Polym Sci.* 1995;20:651–701.
28. Ziani N, Belhadji M, Heireche L, Bouchaour Z, Belbachir M. Crystallization kinetics of $\text{Ge}_{20}\text{Te}_{80}$ chalcogenide glasses doped with Sb. *Phys B.* 2005;358:132–7.
29. Ozawa T. A new method of analyzing thermogravimetric data. *Bull Chem Soc Japan.* 1965;38:1881–6.
30. Augis JA, Bennett JE. Calculation of the Avrami, parameters for heterogeneous solid state reactions using modification of the Kissinger method. *J Therm Anal.* 1978;13:283–92.
31. Vázquez J, Gonzalez-Palma R, Villares P, Jimenez-Garay R. Theoretical study on the glass-crystal transformation and deduction of its kinetic parameters by DSC, using non-isothermal regime. *Phys B.* 2003;336:297–307.
32. Ray CS, Fang X, Day DE. New method for determining the nucleation and crystal growth rates in glasses. *J Am Ceram Soc.* 2000;83:865–72.
33. Noguera O, Merle-Mérjean T, Mirgorodsky AP, Smirnov MB, Thomas P, Champarnaud-Mersjard JC. Vibrational and structural properties of glass and crystalline phases of TeO_2 . *J Non-Cryst Solids.* 2003;330:50–60.
34. Blanchandin S, Marchet P, Thomas P, Champarnaud-Mesjard JC, Frit B, Chagraoui A. New investigations within the TeO_2 – WO_3 system: phase equilibrium diagram and glass crystallization. *J Mater Sci.* 1999;34:4285–92.
35. Zhang JJ, Dai SX, Wang GN, Sum HT, Zhang LY, Hu LL. Fabrication and emission properties of $\text{Er}^{3+}/\text{Yb}^{3+}$ codoped tellurite glass fiber for broadband optical amplification. *J Lumin.* 2005;115:45–52.
36. Pratap A, Lad KN, Shanker Rao TL, Majmudar P, Saxena NS. Kinetics of crystallization of amorphous $\text{Cu}_{50}\text{Ti}_{50}$ alloy. *J Non-Cryst Solids.* 2004;345:178–81.
37. Idalgo E, Araújo EB, Yukimitu K, Moraes JCS, Reynoso VCS, Carvalho CL. Effects of the particle size and nucleation temperature on tellurite $20\text{Li}_2\text{O}$ – 80TeO_2 glass crystallization. *Mater Sci Eng A.* 2006;434:13–8.